Deposition Method for Preparing SERS-Active Gold Nanoparticle Substrates

ARTICLE *in* ANALYTICAL CHEMISTRY · DECEMBER 2005

Impact Factor: 5.64 · DOI: 10.1021/ac050437v · Source: PubMed

5 AUTHORS, INCLUDING:

Khee Chee Soo
Duke-NUS Graduate Medical School Singapore
280 PUBLICATIONS **5,194** CITATIONS
SEE PROFILE

Malini Olivo
Agency for Science, Technology and Researc…
278 PUBLICATIONS **4,016** CITATIONS
SEE PROFILE

Anal. Chem. **2005,** *77,* 7462−7471

Technical Notes

Deposition Method for Preparing SERS-Active Gold Nanoparticle Substrates

Kiang Wei Kho,[†,‡] Ze Xiang Shen,[‡] Hua Chun Zeng,[§] Khee Chee Soo,[†] and Malini Olivo*[,†]

Division of Medical Sciences, National Cancer Centre, 11 Hospital Drive, 169610, Singapore, Department of Physics, and Department of Chemical and Biomolecular Engineering, Faculty of Engineering, National University of Singapore, Lower Kent Ridge Road, Singapore

Surface-enhanced Raman scattering or SERS, discovered some 20 years ago, has recently become a promising tool for routine biofluid assays in a clinical setting. Many attempts have been made to produce cheap and reproducible SERS-active substrates. In this study, we report on the fabrication of SERS-active substrates through the convective assembly of gold (Au) particles on electrostatically charged glass slides. We show that, by a proper control of the initial particle concentration in an evaporating Au suspension droplet, it is possible to obtain a closely packed colloidal film capable of generating SERS activity. Finally, AFM and SERS measurements of the resulting films reveal comparability in performance with previous silane-immobilized Au colloidal films. The minimum electromagnetic enhancement factor of our films is estimated to be about 2×10^4.

Surface-enhanced Raman scattering (SERS) has been extensively studied since Van Duyne and Creighton's discovery of Raman scattering enhancement of molecules adsorbed on roughened metallic surfaces some 20 years ago.[1−6] Subsequent experimental and theoretical studies have attributed this observation to the light-induced surface plasmon resonance (SPR) on the metallic surfaces. The result of SPR is the creation of "hot" electric field spots on the curved surfaces as well as in the troughs between nanoprotrusions.[7] Consequently, molecules that are trapped within or situated in the vicinity of these "hot" zones would experience a strong excitation field and in turn emit amplified Raman intensities.[2] Experimental and theoretical studies have shown that an enhancement in the order of from 10^3 to 10^6 is attainable in SERS,[8] giving a detection limit up to the subpicogram range.[8,9] As such, SERS has recently become a promising analytical tool in the medical field[1] and has been used for the study of trace analytes (e.g., urea, critic acid) and chemical changes in blood and urine.[10,11]

For all the SERS-active metallic surfaces that have been developed and studied, it has been amply demonstrated that surfaces consisting of closely packed but not aggregated colloidal arrays are particularly enhancing, owing primarily to the interparticle plasmon resonance.[6] Thus, many attempts have been made to prepare closely packed colloidal films. Currently, available fabrication techniques encompass vapor deposition of nanoparticles on silica posts,[12] fabrication of periodic arrays of nanoparticles via nanosphere lithography,[13] electron beam lithography,[14] self-assembly of nanoparticles on a chemically functionalized solid surface,[6] and silver enhancement of seed particles that have been predeposited on glass substrates.[15] While these substrates have been shown to exhibit large Raman enhancement and good SERS reproducibility, most are, unfortunately, too laborious and expensive to fabricate in large quantities. For instance, nanosphere lithography requires the use of a thermal evaporator equipped with an accurate thickness monitor so as to ensure proper deposition thickness of metal over the nanosphere mask precoated on the substrate.[6] Electron beam lithography is an alternative,[14] but this is expensive and labor intensive. To this end, Grabar and co-workers have devised a simpler and cheaper approach in which

[†] National Cancer Centre.
[‡] Department of Physics, National University of Singapore.
[§] Department of Chemical and Biomolecular Engineering, National University of Singapore.

(1) Jeanmaire, D. L.; Van-Duyne, R. P. *J. Electroanal. Chem.* **1977**, *84*, 1−20.
(2) Albrecht, M. G.; Creighton, J. A. *J. Am. Chem. Soc.* **1977**, *99*, 5215−5217.
(3) Bjernald, E. J.; Foldes-Papp, Z.; Kall, M.; Rigler, R. *J. Phys. Chem. B* **2002**, *106* (6), 1213−1218.
(4) Mulvaney, P.; He, L.; Natan, M. J.; Keating, C. D. *J. Raman Spectrosc.* **2003**, *34* (2), 163−171.
(5) Podstawka, E.; Ozaki, Y.; Proniewicz, L. M. *Appl. Spectrosc.* **2004**, *58* (5), 570−580.
(6) Grabar, K. C.; Freeman, R. G.; Hommer, M. B.; Natan, M. J. *Anal. Chem.* **1995**, *67* (4), 735−743.
(7) Sanchez-Gil, J. A.; Garcia-Ramos, J. V.; Mendez, E. R. *Opt. Express* **2002**, *10* (17), 879−886.
(8) Van-Duyne, R. P.; Kurt, L. H.; Robert, I. A. *Chem. Phys. Lett.* **1986**, *126*, 190−196.
(9) Dou, X.; Takama, T.; Yamaguchi, Y.; Yamamoto, H. *Anal. Chem.* **1997**, *69*, 1492−1495.
(10) Oneal, P. D.; Cote, G. L.; Motamedi, M.; Chen, J.; Lin, W. C. *J. Biomed. Opt.* **2003**, *8* (1), 33−39.
(11) Sulk, R.; Chan, C.; Guicheteau, J.; Gomez, C.; Heyns, J. B. B.; Corcoran, R.; Carron, K. *J. Raman Spectrosc.* **1999**, *30* (9), 853−859.
(12) Vo-Dinh, T.; Hiromoto, M. Y. K.; Begun, G. M.; Moody, R. L. *Anal. Chem.* **1984**, *56* (9), 1667−1670.
(13) Haynes, C. L.; Van-Duyne, R. P. *J. Phys. Chem. B* **2001**, *105* (24), 5599−5611.
(14) Felidj, N.; Aubard, J.; Levi, G.; Krenn, J. R.; Hohenau, A.; Schider, G.; Leitner, A.; Aussenegg, F. R. *Appl Phys Lett.* **2003**, *82* (18), 3095−3097.
(15) Li, X.; Xu, W.; Jia, H.; Wang, X.; Zhao, B.; Li, B.; Ozaki, Y. *Appl. Spectrosc.* **2004**, *58* (1), 26−32.

10.1021/ac050437v CCC: $30.25
Published on Web 10/08/2005

nanoparticles are self-assembled on chemically functionalized (with organosilanes) glass surfaces.[6] While this particular technique is relatively simpler, it is unfortunately compromised by the requirement that the glass slides be thoroughly cleaned with a highly oxidizing cleaning solution (e.g., piranha solution) before derivatization with colloid can be carried out. Extreme care must be taken when handling the solution as it normally reacts explosively with organic substances such as acetone.[6] Moreover, the solution can also generate toxic waste products, which, in some cases, can be carcinogenic to humans. Last, the solution must be prepared freshly each time, rendering it too costly to scale up for large numbers. As such, we seek to find a safer and cheaper alternative to fabricating SERS-active closely packed colloidal films. More specifically, we ask whether a stable layer of closely packed Au particles can be obtained through the convective assembly of suspended Au colloid. While convection-induced ordered packing of dielectric particles (e.g., latex) with sizes between 42 nm and 1.1 μm has been extensively studied,[16−18] convective assembly of small, charged-stabilized metallic colloids (5−15 nm) has been shown to be more problematic due to the particles' large Hamaker constant,[6,18−22] which makes them relatively unstable. Thus, arrays of closely packed metallic particles can form only if the salt content in the solvent is sufficiently low or completely removed and/or the particle is protected with a layer of surfactant molecules or ions. Examples of a closely packed Au colloidal film would be those reported in the studies by Giersig and Mulvaney[23,24] and Zhao et al.,[21] who deposited Au particles on TEM grids via electrophoretic means and convective assembly, respectively. Unfortunately, as has been pointed out by Michael, colloidal films prepared on TEM grids are not stable and would tend to break or crack during handling, owing to the softness of the grid.[24] Furthermore, particles adsorbed on these grids could be resuspended very easily, since they are not immobilized chemically.[23] As such, the above colloidal films are unapt for SERS applications. On the other hand, Prevo and Velev studied the deposition of a metallic colloidal layer on a solid glass substrate via convective assembly of 15 nm Au suspension in the wetting film of a moving meniscus.[18] Yet, in contrast to Zhao et al.'s report, Prevo and Velev did not observe any organized lattice or closely packed particles; instead the particles formed micrometer-sized aggregates with ill-defined dimensions,[18] which is likely a result of high particle concentration in the colloid meniscus.

Here, we show that through a proper control of the initial particle concentration in a drying colloidal droplet, it is possible to obtain a stable, closely packed colloidal film capable of SERS activity. In addition, we use an electrostatically charged glass slide as the supporting substrate. This allows the Au particles to be firmly immobilized via electrostatic attraction forces, thereby significantly improving the film's stability and hence the SERS performance. No oxidizing cleaning solution is needed in this case as the glass slide used here is a commercially available product. Uniform particle layers can be readily identified after the solvent has completely evaporated. A comparison of the AFM micrographs for our films and those previously reported for chemically immobilized colloidal films reveals qualitatively similar surface morphology in that the majority of the constituent particles are closely packed but not aggregated. Subsequent SERS measurements of our films showed comparable SERS reproducibility and enhancement factor to those chemically immobilized colloidal films. Therefore, we believe that our deposition technique may be the simplest alternative for preparing SERS-active substrates.

EXPERIMENTAL SECTION

Materials. A 15 nm Au hydrosol (EMGC.15, particle concentration = 1.4×10^{12} particles per mL, %CV < 10%) was purchased from British Bio-cell International and used as received. This colloid was stored at 4 °C if not in use. Ethanol was purchased from Merck. Distilled water (18 MΩ) was obtained from a Millipore Mili-Q water purification system. SuperFrostPlus microscope glass slides were purchased from VWR Scientific. Plastic containers for saliva collection (15 mL) and centrifuge tubes (1.5 mL) were purchased from Eppendorf. Crystal violet (CV) was purchased from Sigma-Aldrich and silica gel from Chemicod.

Au Hydrosol Preparation. Au hydrosols containing different particle concentrations were prepared as follows: To increase the particle concentration to 1.9×10^{12} particles per mL, 1 mL of the Au hydrosol was pipetted into a 2 mL centrifuge tube and spun at 14 000 rpm for 5−10 min. About 300 μL of the supernatant was then discarded before resuspending the Au particles with a vortex mixer. To decrease the particle concentration to 3.5×10^{11} particles per mL, 250 μL of the Au hydrosol was pipetted in a 2 mL centrifuge tube, and then distilled water was added to a final volume of 1 mL.

SERS Substrate Preparation. SuperFrostPlus microscope glass slides were rinsed thoroughly with 70% v/v aqueous solution of ethanol for 1 min. The slides were then rinsed 4 times, to remove traces of ethanol, with fresh distilled water each time. The slides were stored in water until needed. To fabricate a Au colloidal film, a Au hydrosol droplet of about 150 μL in volume was pipetted onto the surface of a cleaned slide. The slide was subsequently dried in a desiccator for 24 h, followed by vigorous rinsing in distilled water, and finally dried with a dust blower. All of the prepared Au colloidal films were then kept in distilled water or a dust-free environment until needed.

Preparation of CV Solutions. CV solutions with concentrations of 1 μM, 100 μM, and 1 mM were prepared in phosphate-buffered saline (PBS) pH 7.2.

Instruments. Optical transmission measurements of the resultant Au colloidal films were performed using a Shimadzu UV-2401 PC monochromator system. A cleaned SuperFrostPlus microscope slide was used as the reference sample. Each slide bearing a Au film was placed in the illumination light path and secured with blue-tack. The light beam was passing through the slide perpendicularly. Care was taken to ensure that the blue-tack was not in the light path.

Atomic force microscopy (AFM) measurements were performed under ambient conditions using a Digital Instrument

(16) Micheletto, R.; Fukuda, H.; Ohtsu, M. *Langmuir* **1995**, *11*, 3333−3336.
(17) Ng, V.; Lee, Y. V.; Chen, B. T.; Adeyeye, A. O. *Nanotechnology* **2002**, *13*, 554−558.
(18) Prevo, B. G.; Velev, O. D. *Langmuir* **2004**, *20* (6), 2099−2107.
(19) Dimon, P.; Sinha, S. K.; Weitz, D. A.; Safinya, C. R.; Smith, G. S.; Varady, W. A.; Lindsay, H. M. *Phys. Rev. Lett.* **1986**, *57*, 595−598.
(20) Weitz, D. A.; Lin, M. Y.; Sandroff, C. J. *Surf. Sci.* **1985**, *158* (1−3), 147−164.
(21) Zhao, S.-Y.; Wang, S.; Kimura, K. *Langmuir* **2004**, *20* (5), 1977−1979.
(22) Diao, J. J.; Qiu, F. S.; Chen, G. D.; Reeves, M. E. *J. Phys. D: Appl. Phys.* **2003**, *36* (3), L25 − L27.
(23) Giersig, M.; Mulvaney, P. *Langmuir* **1993**, *9* (12), 3408−3413.
(24) Giersig, M.; Mulvaney, P. *J. Phys. Chem.* **1993**, *97* (24), 6334−6336.

DI3000 Nanoscope III in tapping mode (247.9 kHz) with a typical lateral and vertical resolution of about 5 and 1 nm, respectively. The horizontal scanning rate is 1 Hz.

The Raman experiments were carried out with a modified micro-Raman system, in which an Olympus microscope with a color closed circuit television (CCTV) system is coupled to a Spex 1704 spectrometer that is equipped with a liquid nitrogen cooled CCD detector.[25] In this modified system, the coupling optics are arranged in a box that is linked to the modified optical microscope by a mechanical arm and fixed to the Spex spectrometer. The laser light (632.8 nm) is introduced from the back of the box, after passing through a plasma filter, and is then directed into a microscope via a notch filter, which acts as a reflection mirror to the laser light, but to the signal returning from the sample, it acts as a very effective rejection filter to the Rayleigh (laser) line. This filter prevents any backscattered laser from entering the spectrometer, and hence from interfering with the Raman signals to be collected, but allows Raman signals to transmit with little attenuation. The returned signals then pass through a second notch filter which is used to further improve the Rayleigh rejection. The Raman signal is then focused onto the entrance slit of the Spex spectrometer by a coated singlet focusing lens of 50 mm focal length. The inclusion of the CCTV system allows both the laser beam and white light to be viewed directly from the monitor. A biological specimen can also be viewed directly from the monitor. A 20 × 0.4 NA objective lens purchased from Olympus was used in this study.

SERS Measurements. A droplet (approximately 30 μL) of a CV solution is pipetted onto a dried Au colloidal film. By adjusting the microscope stage, the 633 nm laser was focused, via a 20 × 0.4 NA objective lens, through the sample solution and onto the sample−film interface. Spectrum acquisition was then started immediately. Laser intensity at the focal spot was about 2 mW. The spectral resolution was 1 cm^{-1}, and an integration time of 20 s was used for all Raman measurements.

The focus spot size was defined as the area enclosed by the first dark ring of the airy disk, the diameter of which can be calculated using the formula, $1.22\lambda/\eta \sin\alpha$,[26] where λ is the laser wavelength, η is the refractive index of the solvent, and α is the half-angle of the focusing light cone. The diameter and area of the focus spot are 1.48 μm and 1.72 μm^2, respectively.

Unenhanced Raman Measurements. A droplet (approximately 30 μL) of a 100 μM CV solution is pipetted onto a cleaned microscope glass slide. By adjusting the microscope stage, the 633 nm laser was focused, via the objective lens, onto the liquid surface of the droplet. Spectrum acquisition was then started immediately. Laser intensity at the focal spot was 2 mW. The spectral resolution was 1 cm^{-1}, and the integration time was 20 s.

Again by making use of the diffraction theory, we calculated a probe volume of about 15 fL at the focus. Therefore, about 1.5 × 10^{-18} mol (15 fL × 100 μM) of CV molecules was being probed in the unenhanced Raman measurements.

RESULTS AND DISCUSSION

Macroscopic and Microscopic Characterization of Au Colloidal Films. Metal colloidal substrates containing layers of closely packed particles are normally SERS-active.[6,15,27,28] They derive their SERS activity mainly from the crevices between two adjacent particles, in which trapped analyte molecules experience enhanced electromagnetic field due to interparticle surface plasmon resonance.[3,29−31] A number of methods have been devised to achieve close particle spacing as discussed earlier.[4,6,15,27,28] In this study, we investigate colloidal films deposited by evaporating Au suspension droplets on electrostatically charged glass slides. The typical image of circular colloidal films obtainable when the solvent has completely evaporated is shown in Figure 1a. These films exhibit a characteristic "coffee-ring" feature. A magnified image, taken using a stereomicroscope, of a portion of the one of the films is shown in Figure 1b. One can clearly see two distinct features, a ring and a uniform colloidal Au layer, indicating that there are two different stages in the evaporation process. Initially, the ring is formed when the contact line (the intersection at which the droplet surface touches the solid substrate) is pinned down by nanoparticles jammed between the liquid surface and the glass surface. Since the contact line cannot shrink at this stage, an outward flow of liquid from the interior is induced, as a result, to replenish the evaporative losses along the perimeter of the droplet.[18,32−34] Owing to the viscosity of the solvent, the flow carries the suspended particles toward the pinned contact line, bringing about accumulation of particles there, i.e., ring formation. But as the volume of the drying droplet continues to reduce so does the contact angle. Eventually, the surface tension will balance out the pinning force, causing the contact line to pull off from the ring. This is the start of the second stage, where the contact line slowly retracts toward the drop center, creating a continuous colloidal layer that extends from the ring deposit. We shall show later that by properly controlling the initial particle concentration in the drying droplet, a closely packed but nonaggregated colloidal layer can be obtained. Note that the deposit pattern observed in the current experiment is consistent with that reported by Deegan et al. in their study of dried liquid droplets containing small latex beads.[33]

Further analysis of our films shows that a good film reproducibility is attainable with the current deposition technique. One can readily obtain a uniform colloidal film of at least 6 mm^2 in size. This can be seen from Figure 1b. Note that the image has been processed to correct for any intensity variation arising from uneven illumination over the imaged area. From the histogram shown in Figure 1c, the mean intensity of the enclosed area is calculated to be 198.66 (mean background intensity = 206.94) with a standard deviation (STD) of about 2.92, which is comparable to the 2.41 calculated for the uncoated glass surface (on the left of the ring). We attribute these low STD values to noise in the image. A large

(25) Qin, L.; Shen, Z. X.; Tang, S. H.; Kuok, M. H. *Asian J. Spectrosc.* **1997**, *1*, 121.

(26) Max, B.; Emil, W. *Principles of Optics*; Pergamon Press: London, 1964.

(27) Olson, L. G.; Lo, Y.-S.; Beebe, T. P., Jr.; Harris, J. M. *Anal. Chem.* **2001**, *73*, 4268−4276.

(28) Zhang, J.; Li, X.; Liu, K.; Cin, Z.; Zhao, B.; Yang, B. *J. Colloid Interface Sci.* **2002**, *255*, 115−118.

(29) Mabuchi, M.; Takenaka, T.; Fujiyoshi, Y.; Uyeda, N. *Surf. Sci.* **1982**, *119* (2−3), 150−158.

(30) Blatchford, C. G.; Campbell, J. R.; Creighton, J. A. *Surf. Sci.* **1982**, *120* (2), 435−455.

(31) Ahem, A. M.; Gavell, R. L. *Langmuir* **1995**, *7* (2), 254−261.

(32) Robert, J. G. *Contact Angle, Wettability, and Adhesion*; Fawkes, F. M., Ed.; Advances in Chemistry Series 43; American Chemical Society: Washington, DC, 1964; p 112.

(33) Deegan, R. D.; Bakajin, O.; Dupont, T. F.; Huber, G.; Nagel, S. R.; Witten, T. A. *Nature* **1997**, *389*, 827−829.

(34) Deegan, R. D. Ph.D. Thesis in Physics, University of Chicago, 1998; p 40.

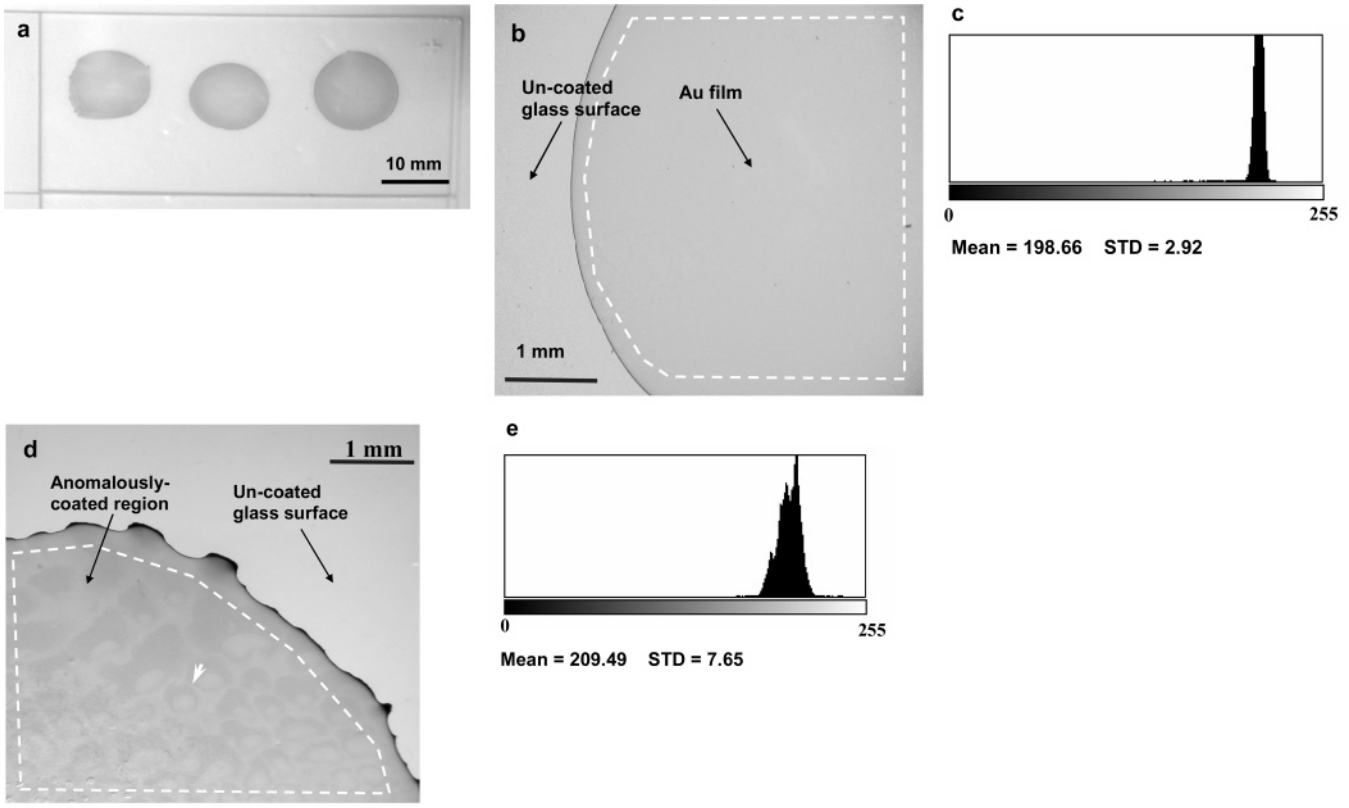

Figure 1. Macroscopic and microscopic images of colloidal films fabricated by drying 150 μL of 15 nm Au suspension droplet on a SuperFrostPlus microscope slide. (a) Macroscopic image showing three colloidal films. (b) Magnified view showing a portion of one of the films. (c) Histogram of the enclosed area shown in (b). (d) Magnified image of an unevenly coated area showing archlike structures. (e) Histogram of the closed area shown in (d). Note that both images shown in (b) and (d) have been processed to correct for intensity variations arising from uneven illumination over the imaged area.

uniform colloidal region means ease of identification and localization of areas for carrying out SERS measurements. We will hereby refer to such a uniform colloidal region as the microscopically uniform colloidal area.

Also of interest are the inevitable anomalously coated regions present in some of the films fabricated. A representative microscopic image of such regions is shown in Figure 1d. One can notice archlike structures (arrowed). Although surfactant-enhanced Bernald convection can also give rise to a similar structure,[35] we believe a different mechanism has taken place here since the arches are not connected as in the case observed in ref 35. One plausible explanation is that as the contact line retreats, different segments along the line move at different speeds, resulting in convex and concave regions: segments that move slower become convex, while those that move faster become concave. Consequently, the convex region would deposit faster than the concave region,[33] thereby forming a semiring or arch. Exactly how and when the contact line starts to move in this fashion is not known at this stage, but it is suspected to have begun at the very initial stage of the evaporation process along regions where the contact line is irregular. This is quite telling since irregular ring deposits are often found near regions containing archlike structures (compare the ring deposits in Figure 1, parts b and d). The exact mechanism behind the formation of such an interesting pattern is currently being investigated.

(35) Van, X. N.; Kathleen, J. S. *Phys. Rev. Lett.* **2002**, *88* (6), 164501−164504.

Figure 1e shows a histogram derived for an anomalously coated region (the enclosed region in Figure 1d). The mean intensity is 209.49 with a STD of 7.95, which is about 3 times as large as that of the uniform Au colloidal film.

Surface Morphologies of Au Colloidal Films. As mentioned above, we are interested in what the effect of the initial particle concentration of the drying droplets would have on the surface morphology of the microscopically uniform colloidal areas. In particular, we would like to know the optimal particle concentration for generating a colloidal array consisting of closely spaced but physically separated particles. To this end, droplets containing different particle concentrations were dried as delineated above. Generally, we did not find any significant difference in the general feature of the resulting films (a ring deposit along the perimeter of the films, a uniform-coated region extending from the ring, and some regions containing archlike structures) except that those derived with lower particle concentrations appear more translucent and pinkish. The optical properties of the microscopically uniform colloidal areas are studied using UV−vis spectroscopy. Typical UV−vis spectra are shown in Figure 2. Note that we have taken care to ensure that only the uniform areas are illuminated and have also confirmed that the ring deposit around each film is not contributing any detectable effect on the final spectrum. Thus, the spectra shown for the films directly reflect the surface properties of the uniform colloidal layers. The UV−vis spectrum for a solution containing isolated 15 nm diameter colloidal Au

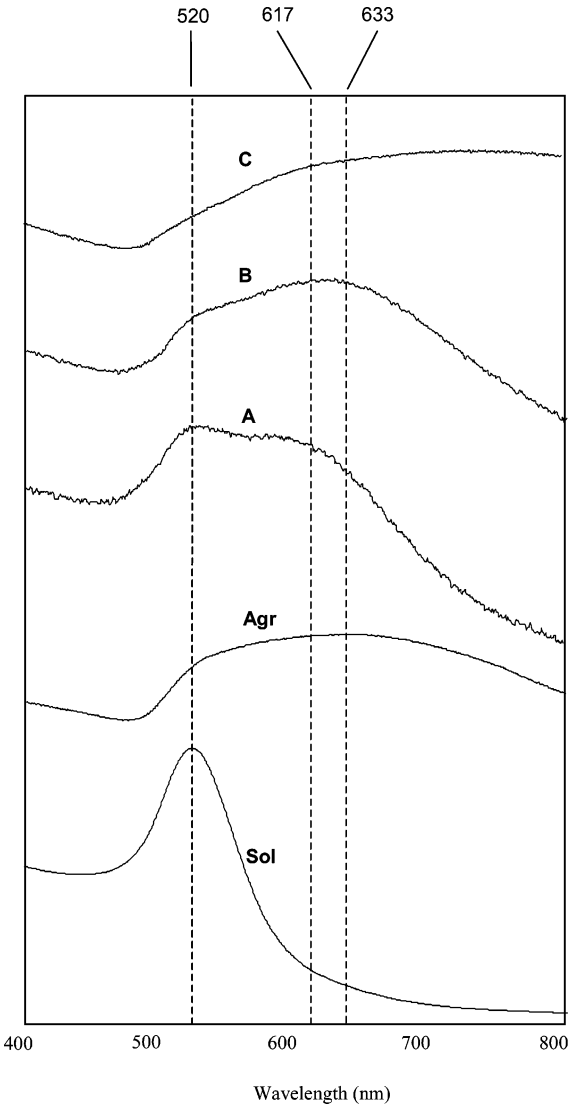

Figure 2. Normalized UV−vis spectra. Sol: 15 nm Au hydrosol; Agr: solution containing Au aggregates induced by mixing NaCl with Au hydrosol. A, B, and C: Normalized UV−vis spectra of dried colloidal films prepared from droplets containing 3.5×10^{11}, 1.4×10^{12}, and 1.9×10^{12} particles per mL, respectively. Curves are shifted vertically for clarity.

particles (spectrum denoted as sol) and that for a solution of Au aggregates induced by addition of 10% NaCl to the Au hydrosol (spectrum denoted as Agr) are also shown for comparison. As can be seen, there are distinct differences between the spectrum derived from the isolated Au particles and those from the other samples. This is due mainly to the different levels of coupling between particles. In the isolated sol, which has a particle concentration of 1.4×10^{12} particles per mL, the average particle separation is estimated to be about 900 nm ($\gg$15 nm). With such a large separation, interparticle coupling is extremely weak, and the UV−vis spectrum is predominantly derived from the surface plasmon resonance in the individual particles. The physical nature of this resonance mode, which gives the colloidal Au its characteristic intense red color, is well understood, as are its dependence on particle size and shape.[29,36] In the current case, this resonance peak is situated at 520 nm, which is in agreement with the previous results obtained for a 15 nm spherical Au colloid.[6] However, when the interparticle separation is comparable to the particle diameter ($\ll\lambda$), interparticle coupling becomes pronounced, and this would generate a new red-shifted feature in the optical spectrum centered between 600 and 800 nm. Theoretical and experimental studies have shown that the intensity and peak of this feature scale with the decrease in particle separation,[15,37] and for particles that are physically connected (i.e., aggregated), this feature would become broadened and shifted to a longer wavelength beyond 700 nm (see spectrum Agr). Red-shifted bands are also seen here in the spectra (curve A, B, and C) of the films deposited using different initial particle concentrations. The general trend observed is that the band shifts to a longer wavelength as the initial particle concentration increases, indicating ascending packing density. In spectra C, which is that of the film deposited by drying colloid droplets containing 1.9×10^{12} particles per mL, the red-shifted band, which is centered at around 720 nm, is broad, suggesting the formation of aggregates (compare this with curve Agr). On the contrary, spectra A and B, which are derived from films fabricated with initial particle concentrations of 3.5×10^{11} and 1.4×10^{12} particles per mL respectively, exhibit two resonance peaks. The first resonance band is independent of the particle concentration and is situated at 520 nm. This band is attributable to the plasmon resonance in the individual isolated particles. The second band arises from the particle−particle resonance and is located at 617 nm for film A and 633 nm for film B. As reported previously,[6,15,27] the presence of such a double-peak feature is an indication of closely spaced morphology. To verify these results, AFM analysis was performed on the above colloidal films. The AFM data are presented in Figure 3. In film A, one can observe closely spaced but amorphously organized particles with an average particle-to-particle separation of about 30 nm, which is in good agreement with the closely packed morphology predicted above from the UV−vis spectrum. As can be seen from the height profile, the film thickness is a submonolayer with height variations comparable to the size of the individual particles. Increasing the particle concentration of the evaporating droplets increases the packing density of the resultant colloidal films. This is shown in Figure 3, parts b and c, which correspond to colloidal layers obtained with 1.4×10^{12} and 1.9×10^{12} particles per mL, respectively. One can readily see that, at the highest particle concentration, aggregates of ill-defined dimensions are formed. This correlates well with the UV−vis data described above (see curve C in Figure 2). The surface morphology of the film deposited at an intermediate particle concentration (i.e., film B), on the other hand, is qualitatively different and is interesting in that it consists of interconnected islands. These islands appear to have a "flat top" in general as indicated by the height profile (lower panel in Figure 3b). We thus ask whether these islands are actually domains of closely packed particles that are too small to be resolved by the AFM tip. To answer this question, we digitally improve the lateral resolution of the image by making use of a band-pass filter as described in ref 16. The processed image of the area enclosed by the white-dotted box shown in Figure 3b is presented in Figure 4. Individual particles are now more discernible. One can observe

(36) Bohren, C. F.; Huffman, D. R. *Absorption and Scattering of Light by Small Particles*; John Wiley and Sons: New York, 1983.

(37) Zhao, L.; Kelly, K. L.; Schatz, G. C. *J. Phys. Chem. B* **2003**, *107* (30), 7343−7350.

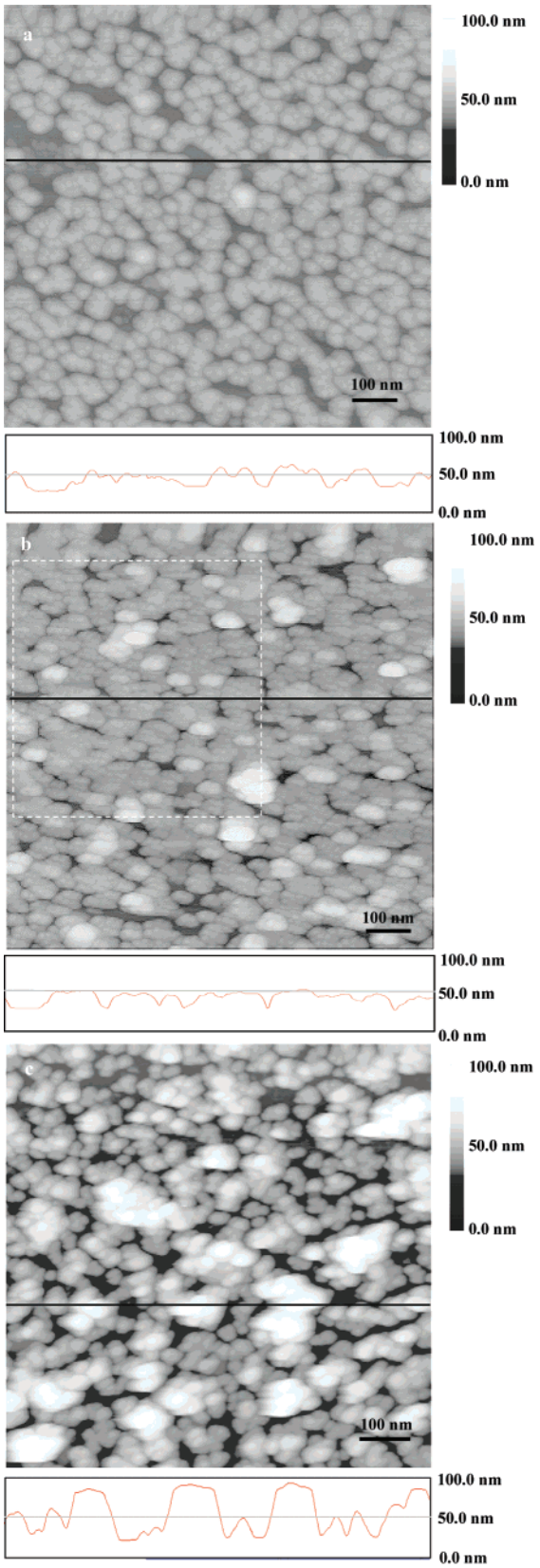

Figure 3. AFM mappings of colloidal films prepared from droplets containing (a) 3.5×10^{11}, (b) 1.4×10^{12}, and (c) 1.9×10^{12} particles per mL. Scanned area = 1 μm × 1 μm.

hexagonal or square particle arrangements (enclosed in dotted boxes). Further analysis of this particular image shows a center-to-center separation ranging between 15 and 17 nm, which is

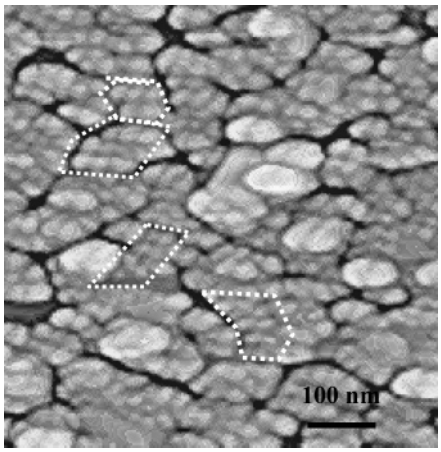

Figure 4. Digitally processed AFM image showing closely packed morphology in the film prepared at an initial particle concentration of 1.4×10^{12} particles per mL.

comparable to the individual particle size. If a particle radius of 7.5 nm (15 nm/2) is assumed, this would be translated into an interparticle spacing of 0−2 nm. Note that this equilibrium distance is far too small to be explained by diffuse-layer repulsion.[24] Thus, the short particle spacing is likely due to the steric interaction of a stabilizing molecular layer adsorbed on the particle surface, in this case, the chloride ions. We have to note that the observation of such a closely packed Au colloidal array, formed by a drying suspension droplet, is rather suprising, because this clearly disagrees with the majority of the previous claims that Au hydrosols are not stable enough to form 2D closely packed colloidal arrays without forming large aggregates,[6,20−22] owing to their large Hamaker constant. Although particles can be made more stable with thiol- and amide-based protection layers to allow the formation of large, ordered 2D colloid lattices, and even 3D superlattices,[38,39−41] capping Au particles with a protective layer may have compromising effects on their SERS performance: first, the protective layer can increase the separation between the absorbate and the particle surface, thereby reducing the SERS effect[3]; second, the protective layer may introduce confounding signals to the final SERS spectrum.[3] However, as far as reusability is concerned, a suitably thin protective layer may still be desirable to prevent covalent bonding of the absorbate on the metal surface. This will be investigated in the future as an improvement to our Au colloidal films.

Film Stability. One of the principal objectives of the current study is to prepare SERS-active substrates that are suitable for biofluid analysis. Since biofluids generally contain a certain amount of salts, it is thus important to study the stability of the Au colloidal layers under conditions of high ionic strengths. To achieve this, we immersed the Au colloidal layers in an aqueous solution containing 10% NaCl, which is about 10 times more salty than

(38) Harfenist, S. A.; Wang, L. Z.; Whetten, R. L.; Vezmar, I.; Alvarez, M. M. *Adv. Mater.* **1997**, *9* (10), 817−822.
(39) Stoeva, S.; Klabunde, K. J.; Sorensen, C. M.; Dragieva, I. *J. Am. Chem. Soc.* **2002**, *124* (10), 2305−231.
(40) He, S.; Yao, J.; Jiang, P.; Shi, D.; Zhang, H.; Xia, S.; Pang, S.; Gao, H. *Langmuir* **2001**, *17* (5), 1571−1575.
(41) Brown, L. O.; Hutchison, J. E. *J. Phys. Chem. B* **2001**, *105*, 8911−8916.

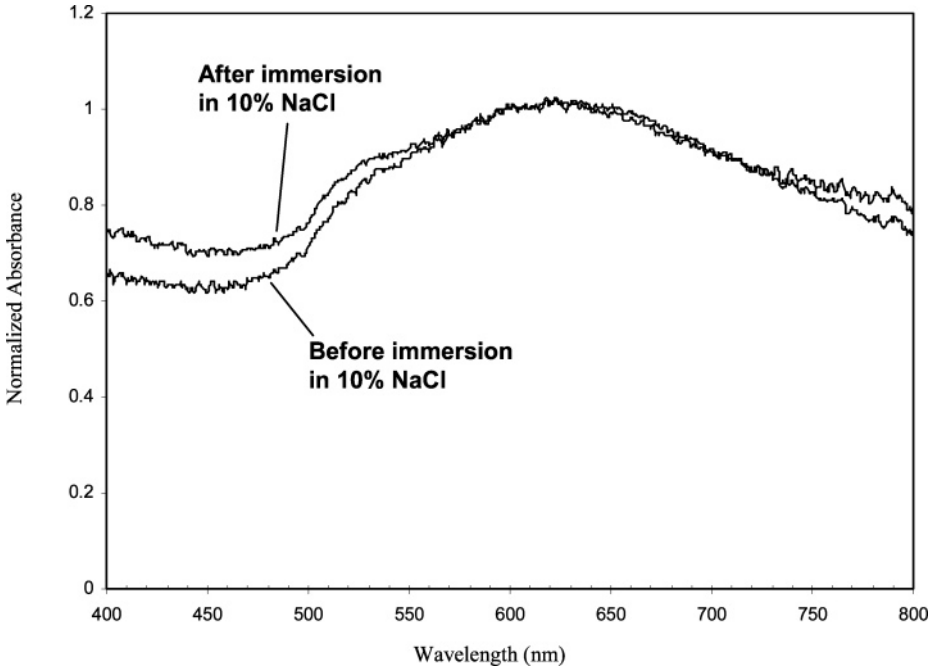

Figure 5. UV−vis spectra of a Au film before and after immersion in a 10% NaCl solution.

the normal physiological levels found in biofluids.[42] No resuspension of particles were observed after 2 weeks. Typical UV−vis absorption spectra measured on these colloidal layers before and after the NaCl treatment are shown in Figure 5. Both spectra are generally identical, indicating that there is no appreciable morphological change in these layers after the treatment. This is clearly in contrast to Au hydrosols, which tend to coagulate at high molarities of salts (see curve Agr in Figure 2) due to the screening of the repulsive interactions between particles by the co-ions. The excellent stability of our films toward salty solutions therefore leads us to believe that the Au particles are bonded firmly via electrostatic interactions to multiple sites on the charged SuperFrostPlus surface. In fact, in order for all of our SERS experiments described below to be of biological relevance, all sample solutions used in the experiments were prepared with a physiological salt concentration of about 0.2 M.

Finally, we have to stress that our films are assembled solely by the convection-induced particle flows in the wetting film near the contact line of the drying droplet and not by spontaneous electrostatic adsorption of particles on the glass surface as in the case of electrostatic self-assembly,[43] since immersing the SuperFrostPlus glass slides in a solution of Au colloid for 2 days did not result in particle attachment. Note also that in no case did we obtain any stable colloidal film if the suspension drops are dried on normal glass slides, which lack the electrostatic layers. Films formed on these slides were either partially or completely removed upon rinsing with distilled water.

Film Reproducibility. A useful deposition method must be reproducible. To this end, we studied the surface roughness of 18 different Au colloidal films fabricated by our deposition method using the initial particle concentration of 1.4×10^{19} particles per mL. This particular concentration was chosen for two main reasons. First, films deposited at this concentration (i.e. film B) have a closely packed surface morphology (see Figure 3b and Figure 4) identical to that of SERS-active silane-immobilized particle arrays.[6,27] Second, UV−vis measurement of the films indicates an interparticle coupling resonance peak at 633 nm, which matches that of our current HeNe excitation laser wavelength, an important criteria for inducing large SERS activity.[44,45] Third, film B has been shown experimentally to be highly Raman enhancing compared to the other two (i.e., films A and C), as will be discussed below.

To quantify film reproducibility, we calculated the arithmetic mean roughness value[46] ($R_s = (1/N)\sum |z_1 - z_{av}|$) for a 1 μm × 1 μm microscopically uniform area in each of the 18 Au colloidal films. An R_s value of 5 nm with a 14% variation was obtained, indicating good reproducible surface roughness. The roughness of the SuperFrostPlus glass surface is measured to be about 0.9 nm and thus does not contribute significantly to the calculated R_s values.

Due to its high Raman enhancement, film B will be used in most of our SERS experiments and will hereby be referred to as the Au film unless otherwise explicitly stated.

Preresonance SERS Spectra of Crystal Violet on Au Films. The SERS performance of the Au films was studied by measuring the Raman signals from CV molecules adsorbed on them. Depending on the solvent's pH, CV generally exists in three different forms.[47] In the present study, the CV was dissolved in a PBS buffer with a pH value of 7.2 and should therefore exist predominantly in the carbonium ion (native) form (chemical structure of which is shown in the inset of Figure 6a). This was confirmed by the occurrence of a prominent singlet $\pi-\pi^*$

(42) Andrei, B.; Elvira, E. M.; Robert, O. D.; Thomas, C. B. *Biochemistry* **1997**, *35* (25), 7821−7831.
(43) Sastry, M. *Pure Appl. Chem.* **2002**, *74* (9), 1621−1630.
(44) Fornasiero, D.; Grieser, F. *J. Chem. Phys.* **1987**, *5*, 3213−3217.
(45) Crieghton, J. A. *J. Chem. Soc., Faraday Trans.* **1979**, *2* (75), 790−798.
(46) Nowicki, B. *Wear* **1985**, *102*, 161−176.
(47) Jessop, J. L. P.; Goldie, S. N.; Scranton, A. B.; Blancherd, G. J. *J. Vac. Sci. Technol., B* **2002**, *20* (1), 219−225.

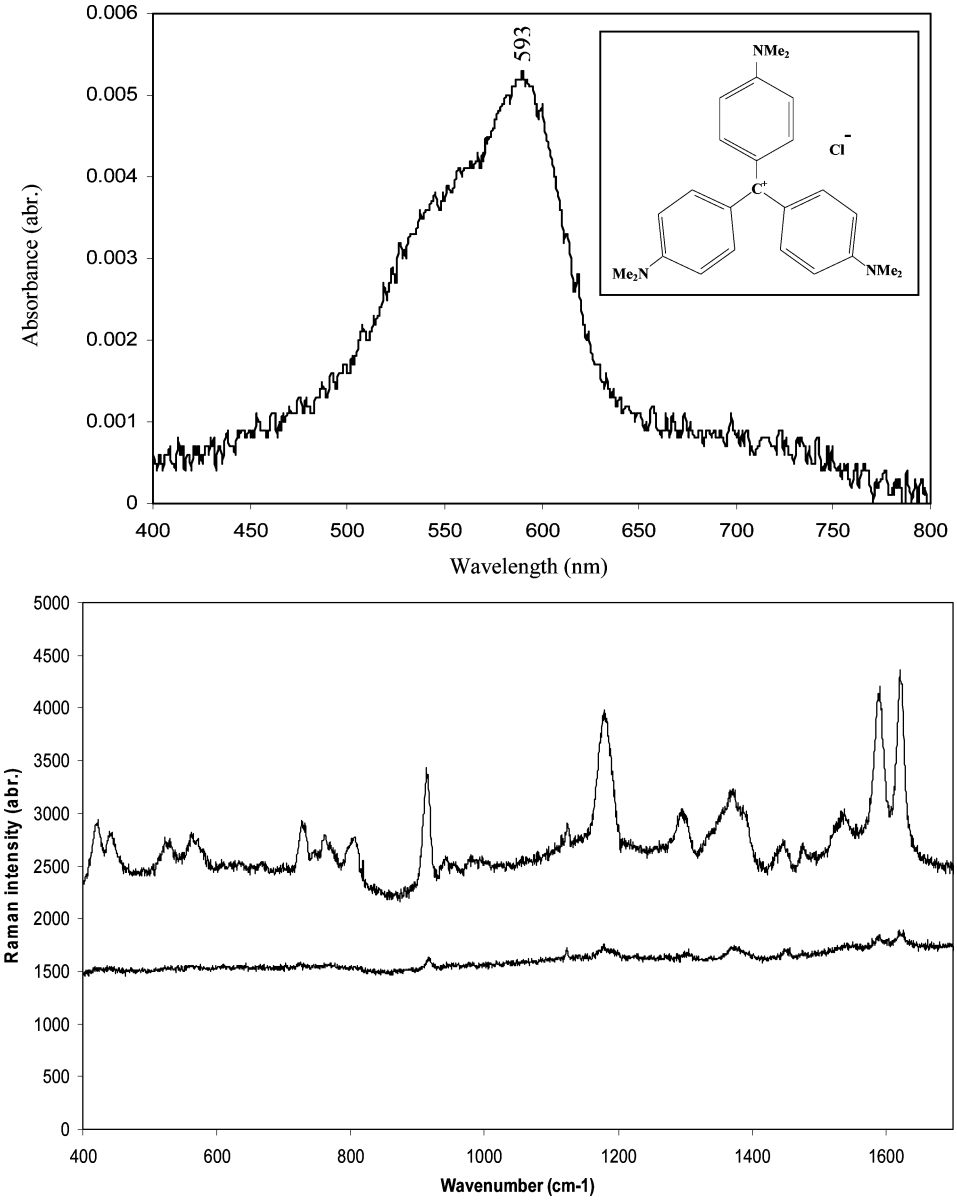

Figure 6. (a) UV−vis spectra of a 1 μM CV solution. Inset: chemical structure of a native CV. (b) Preresonance SERS spectrum of a 1 μM CV solution in pH 7.2 PBS buffer (upper). Unenhanced preresonance Raman spectrum of a 100 μM CV solution in pH 7.2 PBS buffer (lower). Excitation Source: 633 nm; 2 mW; 20 s integration.

electronic absorption peak at 593 nm in the UV−vis spectrum of the CV solutions (see Figure 6a).[47] Thus, at the excitation wavelength of 633 nm, the CV is preresonantly excited.

Typical unenhanced (bottom curve) and surface-enhanced (upper curve) preresonance Raman spectra of CV are shown in Figure 6b. The unenhanced Raman spectrum was derived from the liquid surface of a droplet containing 100 μM CV in PBS, as delineated in the Experimental Section. The preresonance SERS spectrum on the other hand was derived from the surface of a Au film immersed in a 1 μM CV solution. The integration time used for all experiments is 20 s. Note that the use of a buffer solvent is essential. This is to eliminate any pH-dependent variation in the CV's SERS spectrum.[48] The preresonance SERS spectrum obtained here is in good agreement with that previously reported for this particular compound.[48]

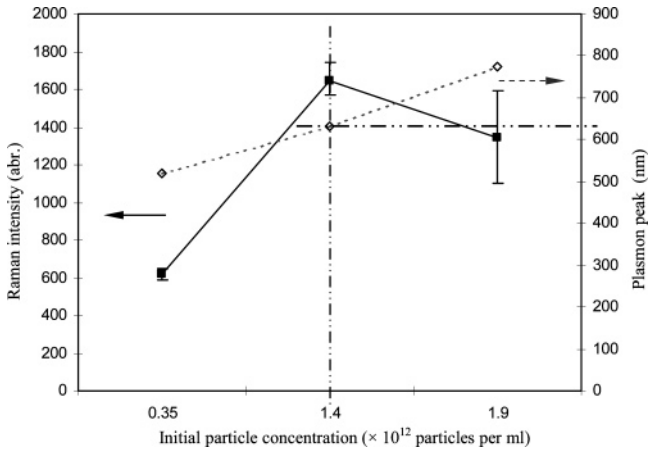

Figure 7. The maximum SERS intensity at 1619 cm^{-1} (left axis, solid line) and the wavelength of the interparticle plasmon resonance (right axis, dashed line) vs the initial particle concentrations.

(48) Polwart, E.; Keir, R. L.; Davidson, C. M.; Smith, W. E.; Saddler, D. A. *Appl. Spectrosc.* **2000**, *54* (4), 522−527.

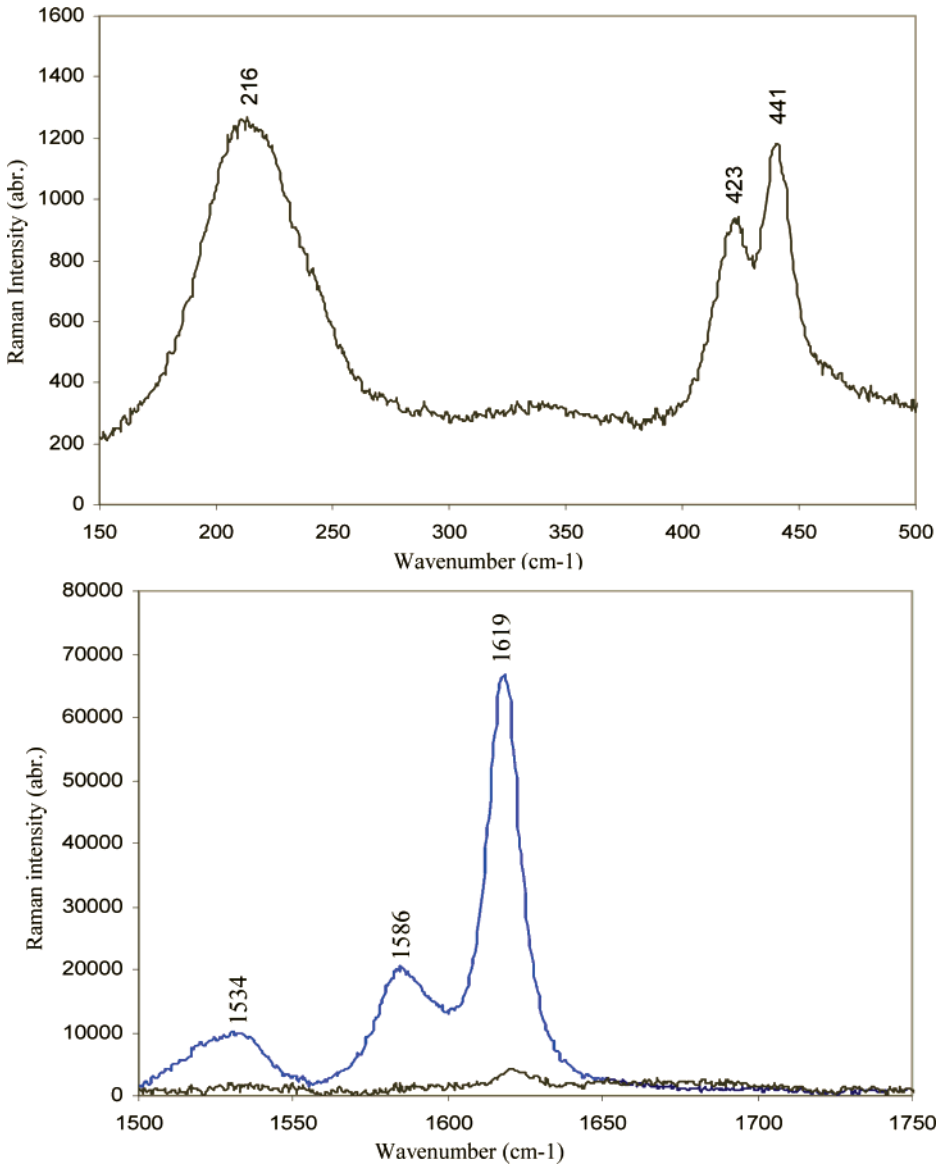

Figure 8. (a) Preresonance SERS spectrum of a 1 μM CV solution in the region of 150−500 cm^{-1}. (b) Preresonance SERS spectrum obtained from a Au film soaked in 1 mM CV solution for 21 h. Excitation Source: 633 nm; 2 mW; 20 s integration.

On the basis of a triplicate measurement of the 1 μM CV's SERS intensities at 1619 cm^{-1}, the SERS reproducibility of our Au films was estimated to be around 14%, which is comparable to that of a silane-immobilized Au colloidal layer.

We also investigated the enhancement of Raman scattering for the Au colloidal arrays fabricated with different initial particle concentrations exposed to a 1 μM CV solution. Generally, the excitation wavelength for the maximum SERS enhancement would coincide with the adsorption maximum of the interparticle plasmon resonance.[44,45] Such a correlation is studied here for our Au colloidal arrays. Figure 7 illustrates the maximum SERS intensity at 1619 cm^{-1} (left axis) and the wavelength of the interparticle plasmon resonance maximum (right axis) versus initial particle concentrations. It can be seen from Figure 7 that the SERS intensity increases with the increase in the initial particle concentrations and then levels down gradually beyond 1.4×10^{19} particles per mL as the interparticle plasmon adsorption maximum shifts to a longer wavelength than the excitation wavelength (633 nm). That is to say, when the wavelength of the plasmon resonance is shorter than the excitation wavelength, the SERS intensity increases with the initial particle concentrations. When the resonance maximum shifts to a wavelength longer than that of the excitation, the SERS intensity falls off. Olson et al. have also found this trend in their research on a silane-immobilized Au colloidal film as a SERS-active substrate.[27]

Raman Enhancement Factor. The apparent enhancement factor (AEF) for the Au films can be calculated by ratioing the intensity of the peak at 1619 cm^{-1} in the preresonance SERS spectrum to that of the corresponding peak in the unenhanced Raman spectrum, taking into account that the SERS signal is derived from a CV solution 100 times more dilute than that used for the unenhanced Raman measurement. According to the curves displayed in Figure 6b, this yields an AEF of approximately 2000.

Unfortunately, it is not as easy to estimate the chemical/electromagnetic enhancement factor of the Au films, since this will generally require a detailed knowledge of the surface morphology, the binding characteristic (i.e., covalent or noncovalent), and the binding geometry of the absorbate on the metallic

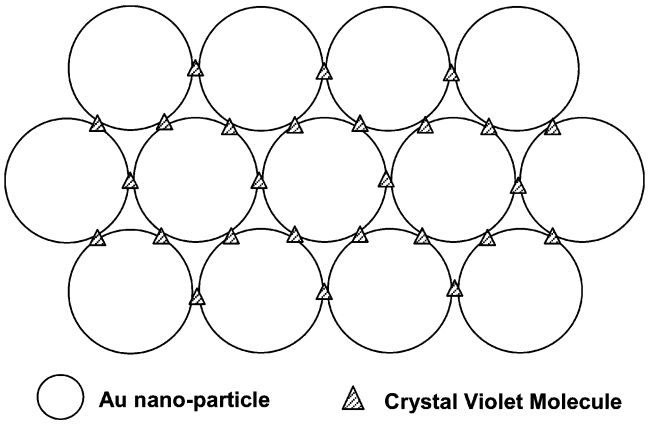

Figure 9. Hexagonally packed Au colloidal array saturated with CV molecules.

surface. As such we can only calculate for the minimum enhancement factor of the Au films. This is achieved in the following manner:

First, we establish that CV molecules are normally bonded to the Au surface by Coulombic and van der Waals interactions.[49] This is evident by the absence of a Au−N stretching vibrational peak in the 225−231 cm^{-1} region of the SERS spectrum derived from Au films exposed to a 1 μM CV solution (see Figure 8a). Clearly, this is in contrast to the SERS spectra of DNA nucleosides chemically adsorbed onto Au nanoparticles, where Au−N peaks were observed indicating that the nucleosides were covalently bonded via the lone electron pair in the nitrogen atoms.[50] We therefore surmise that there is no chemical enhancement in the SERS of the CV−Au complex; i.e., the Raman enhancement observed in the present study is purely electromagnetic. Next, we soak a Au film in a 1mM CV solution for 21 h in an attempt to saturate the film's surface. After rigorous rinsing with PBS solution for 2 min to wash off unbound CV molecules, SERS measurement was carried out immediately with the film remained immersed in the PBS solution. The resultant preresonance SERS spectrum in the region between 1500 and 1750 cm^{-1} is shown in Figure 8b. The intensity of the Raman peak at 1619 cm^{-1} is about 70 000 counts, and further increases in the CV concentration beyond 1 mM did not result in more photon counts, suggesting that a plateau has been reached in the adsorption of CV on the Au film at 1mM. To calculate the *minimum* electromagnetic enhancement factor (EFF), we first made the following assumptions: (1) the Au particles in the array take on a hexagonal packing as shown in Figure 9, which is the maximum packing density possible for a spherical particle; (2) only the molecules that are adsorbed in the crevice ("hot spot") between Au particles needed to be considered since they are the main contributors to the measured SERS signals, as has been reported in the previous electromagnetic studies of SERS;[3,29−31] (3) all available hot spots are occupied by CV molecules when the film is saturated; (4) owing to the large molecular size (120 $Å^2$) of the CV and steric interactions,[51] each hot spot is occupied by not more than one CV molecule (see Figure 9). With these in mind, we then estimated that there are about 3×10^4 SERS-contributing CV molecules ($\sim 5.017 \times 10^{-20}$ mol) residing within the 1.78 μm^2 laser spot. In a similar manner as in the calculation of the AEF, the minimum EEF value is thus calculated to be about 2×10^4. We stress that this is only the lowest estimation, since the surface morphology of the current Au films is not ideally packed and that it is very unlikely that all of the available hot spots between particles are occupied by CV molecules even at very high concentration as has been assumed in the calculation; the actual EEF should thus be significantly higher.

CONCLUSION

We have demonstrated a simple convective assembly of 15 nm Au nanoparticles on electrostatically charged glass substrate. Uniform colloidal layers can be easily found in the dried films and were shown to contain islands of hexagonally spaced particles. The average interparticle separation is estimated to be about 17 nm based on AFM analysis. With the use of CV as a test sample, the SERS reproducibility of a properly deposited films was shown to be about 14%, which is comparable to that previously reported for silane-immobilized Au colloids. The minimum EEF is estimated to be about 2×10^4.

ACKNOWLEDGMENT

We would like to thank Dr. Sow Chorng Haur and Mr. Ong Peng Ming from the Department of Physics, National University of Singapore for their technical assistance with the AFM mapping.

Received for review March 14, 2005. Accepted July 27, 2005.

AC050437V

(49) Liang, J. D.; Burstein, E.; Kobayashi, H. *Phys. Rev. Lett.* **1986**, *57* (14), 1793−1796.
(50) Nak, H. J. *Bull. Korean Chem. Soc.* **2002**, *23* (12), 1790−1800.
(51) Shaw, A. M.; Hannon, T. E.; Li, F.; Zare, R. N. *J. Phys. Chem. B* **2003**, *107*, 7070−7075.